This is an *Accepted Manuscript*, which has been through the Royal Society of Chemistry peer review process and has been accepted for publication.

Accepted Manuscripts are published online shortly after acceptance, before technical editing, formatting and proof reading. Using this free service, authors can make their results available to the community, in citable form, before we publish the edited article. We will replace this *Accepted Manuscript* with the edited and formatted *Advance Article* as soon as it is available.

You can find more information about *Accepted Manuscripts* in the Information for Authors.

Please note that technical editing may introduce minor changes to the text and/or graphics, which may alter content. The journal's standard Terms & Conditions and the Ethical guidelines still apply. In no event shall the Royal Society of Chemistry be held responsible for any errors or omissions in this *Accepted Manuscript* or any consequences arising from the use of any information it contains.

Journal Name

Dynamic Article Links ▶

ARTICLE TYPE

7Carbene Iridium Complexes for Efficient Water Oxidation: Scope and Mechanistic Insights

James A. Woods,[a] Ralte Lalrempuia,[b] Ana Petronilho,[b] Neal D. McDaniel,[a] Helge Müller-Bunz,[b] Martin Albrecht,*[b] Stefan Bernhard*[a]

Iridium complexes of Cp* and mesoionic carbene ligands were synthesized and evaluated as potential water oxidation catalysts using cerium(IV) ammonium nitrate as a chemical oxidant. Performance was evaluated by turnover frequency at 50% conversion and by absolute turnover number, and the most promising precatalysts were studied further. Molecular turnover frequencies varied from 190 to 10 451 per hour with a maximum turnover number of 38,000. While the rate of oxygen evolution depends linearly on iridium concentration, concurrent spectroscopic and manometric observations following stoichiometric oxidant additions suggest oxygen evolution is limited by two sequential first order reactions. Under the applied conditions, the oxygen evolving species appears to be a well-defined and molecular species based on kinetic analyses, effects of careful ligand design, reproducibility, and the absence of persistent dynamic light scattering signals. Outside of these conditions, the complex mechanism is highly dependent on reaction conditions. While confident 15 characterization of the catalytically active species is difficult, especially under high-turnover conditions, this work strongly suggests the primary active species under these conditions is a molecular species.

Broader Context
Large-scale conversion of solar energy into practical fuels requires an intimate understanding of the associated oxygen evolution processes. Water represents an abundant and benign source of molecular oxygen if the reaction thermodynamics and kinetics of oxygen evolving water oxidation processes can be effectively managed. Prior to performing an economic balance of catalyst lifetime and cost, it is necessary to develop a greater understanding of catalytic intermediates and degradation products. The homogeneous reaction conditions of the novel iridium catalyst family presented here enable *in situ* observation of the catalyst speciation and eventually leading to judicious structural modifications that improve catalyst performance and robustness to practical levels.

Introduction

While global demand for energy is projected to increase significantly over the next three decades,[1] estimates for annual total insolation[2] exceed the current and projected global demand for energy by almost four orders of magnitude. Because sunlight is transient, a critical step towards meeting this demand is the effective and efficient transformation of sunlight into a storable source of energy.[3] This issue is highlighted by silicon photovoltaics: despite improvements to cost and capture-efficiency there is currently no lightweight, efficient, and cost-effective way to store the captured solar energy. A more tenable solution would store sunlight in the chemical bonds of a contemporary-compatible fuel.

A photon-driven catalytic cycle could conceivably be tailored to function with any number of well-studied reductive pathways including metal salt to metal,[4] water to hydrogen,[5] and carbon dioxide to methanol.[6] Despite the various potential fuel-producing reductive pathways, complementary oxidative half-reactions producing molecular oxygen are necessary. This simplifies reactant delivery by employing the atmosphere as an oxidant reservoir and conveyance. Water, due to its abundance and benignity, would be an ideal feedstock if not for the complex mechanism and high thermodynamic barrier for the oxidation reaction necessary to produce molecular oxygen.

[a] *Department of Chemistry, Carnegie Mellon University, Pittsburgh, Pennsylvania 15213, United States; E-mail: bern@cmu.edu*
[b] *School of Chemistry & Chemical Biology, University College Dublin, Belfield, Dublin 4, Ireland ; E-mail: martin.albrecht@ucd.ie*

Scheme 1
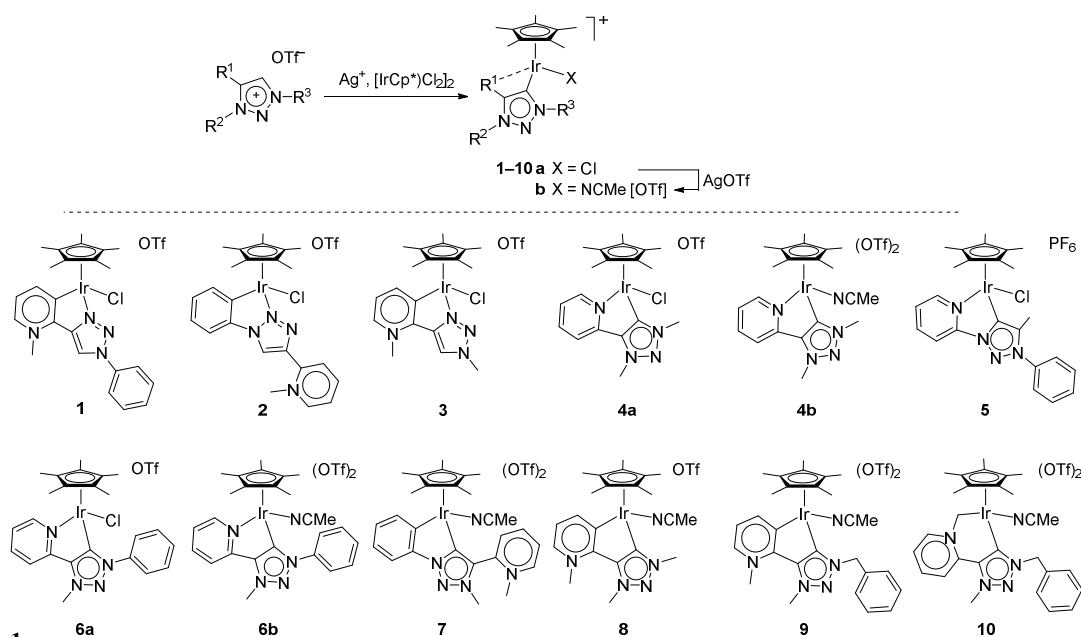
As a tool to understand this complexity, molecular catalysis is one avenue of study yielding the potential for direct characterization, structural tunability, and greater atom economy through homogenous reaction conditions. Citing just a small portion of the broad interest in molecular water oxidation: ruthenium dimers[7–10] and tetramers,[11–13] cobalt tetramers,[14,15] manganese dimers[16] along with work detailing single-site catalysts[17–24] all illustrate the diversity of successful catalysts.

More recently, a variety of Cp*Ir complexes (Cp* = $C_5Me_5^-$) have been shown to act as efficient water oxidation precatalysts.[25–31] These complexes are remarkable for their high activity compared to the original iridium catalysts which featured 2-phenylpyridine ligand spheres. However, mechanistic work under different reaction conditions led to controversial conclusions: while a heterogeneous mode of action has been put forward in some studies,[31–33] support for homogeneous catalysis has been obtained *e.g.* from experiments using a quartz microbalance as a probe and from catalyst immobilization.[33–35] The wide variety of reaction conditions, including the use or absence of organic co-solvents and buffered or unbuffered aqueous catalyst solutions, render direct comparison of results between literature investigations difficult.

Following our initial discovery of triazolylidene iridium complexes as potent water oxidation catalysts, we engaged in careful ligand modification in an attempt to improve catalyst performance and to expand our understanding of oxidation mechanisms with application to a broad variety of fuel producing photosystems.[36–39] Here we report on the synthesis and catalytic activity in water oxidation of an expanded family of cationic Cp*Ir complexes containing either *C,C*-bidentate or a *C,N*-bidentate coordinating carbene iridium complexes.

Results and Discussion

Synthesis and characterization of the complexes

A series of cationic Cp*Ir complexes **1–10** containing either *C,C*-bidentate or a *C,N*-bidentate coordinating chelate was prepared using C–H bond activation chemistry mediated by silver cations (Scheme 1). The type of chelating sites varies considerably from the original C,C bidentate set explored previously.[26] Thus, one set of complexes features chelating *C,N*-bidentate ligands that contain a neutral *N*-bound triazole unit paired with a formally neutral abnormal pyridylidene[40] fragment (C_{pyr}, N_{trz}-bidentate; complexes **1** and **3**) or with an anionic phenyl chelate (C_{aryl},N_{trz}-bidentate; complex **2**). A second set of ligands comprises a triazolylidene core[41,42] with different substitution patterns and an *N*-bound pyridine as chelating group (N_{pyr},C_{trz}-bidentate; complexes **4–6**). *C,C*-Bidentate chelates constitute a further class of ligands, featuring a triazolylidene ligand and an anionic phenyl ligand (C_{aryl},C_{trz}-bidentate; complex **7**), or a triazolylidene and a formally neutral pyridylidene ligand (C_{pyr},C_{trz}-bidentate; complexes **8** and **9**), or an sp³-hybridized ylidic ligand (C_{ylide},C_{trz}-bidentate; complex **10**).

The formation of complexes **1–10** provided some interesting insights into the donor properties of the ligand and the reactivity of the iridium center. In the absence of a chelating nitrogen donor, cyclometalation via C_{aryl}–H bond cleavage took place (*cf* complexes **2**, **7**). Cyclometalation involved exclusively the aryl ring bound to a nitrogen of the heterocyclic core. This reactivity pattern was observed previously also in triazolylidene palladium chemistry[43,44] and suggests an electrophilic bond activation.[45] C_{aryl}–H activation appears to be competitive with $C_{pyridinium}$–H bond activation and the course of the reaction is dependent on whether N2 or N3 of the triazole ring is coordinated to the iridium center (*cf.* formation of a mixture of **1** and **2** from the same ligand precursor).[46] Exchange of the aryl substituent at N1 of the ligand precursor by a methyl group prevents the formation of a chelate via N2 bonding. Consequently, exclusive coordination via N3 and ensuing $C_{pyridinium}$–H bond activation was observed, which afforded the chelating pyridylidene-triazole complex **3**.

All complexes featuring a nitrogen donor ligand were prepared in CH_2Cl_2 and were obtained as monocationic species comprising an iridium-bound chloride ligand. This chloride was readily
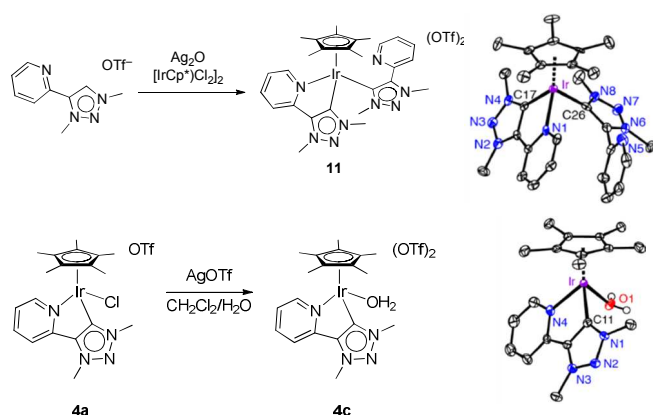
Scheme 2

abstracted by classical methods using AgOTf to yield the dicationic complexes. In contrast, complexes with a *C,C*-bidentate ligand were synthesized in MeCN and were isolated as the dicationic complexes directly from the iridation reaction. This behavior is in line with considerably stronger donor properties of these *C,C*-bidentate ligands compared to their *C,N*-homologues, thus inducing a higher electron density at iridium[47–49] and a destabilization of the putative Ir–Cl bond. The stronger donor properties of such abnormal formally neutral carbene ligands as compared to imines may be rationalized by their pronounced mesoionic character.[50–53] This notion enhances the relevance of a formally anionic carbon bound to the iridium center and a (remote) intermolecular stabilization of the negative charge by an iminium fragment.

Formation of complexes **4–6** with pyridine-functionalized triazolylidenes was straightforward when using equimolar ratios of iridium precursor and triazolium salt. In the presence of (slight) excess of triazolium salts, a second product appeared that was identified as the bis(carbene) complex **11** from two sets of ligand signals in the ^{1}H NMR spectrum in 1:1 ratio. The different shielding of the two sets of pyridyl protons indicates a biscarbene complex **11** comprised of one monodentate, and one *C,N*-bidentate triazolylidene ligand (Scheme 2).[54] Unambiguous confirmation of the formation of complex **11** was obtained from an X-ray diffraction analysis from crystals that grew from a reaction mixture.

The site of metalation in the new complexes **1–8** was readily deduced from NMR spectroscopic analysis of the complexes in CD_3CN solution. N-bound triazole ligands featured a diagnostic low-field signal in the 8.6–9.3 ppm range in the ^{1}H NMR

spectrum due to the presence of the triazole proton at C(5) (complexes **1–3**). Pyridyline-type bonding due to $C_{pyridinium}$–H bond activation was identified by three characteristic resonances at low field (doublets at δ_H 8.7 and 8.3, and doublet of doublets at δ_H 7.6) assigned to the H(4), H(6), H(5) protons respectively of the pyridine heterocycle (complexes **1**, **3**, and **8**). In contrast, four pyridine resonances were clearly distinguishable in complexes featuring N-coordinated pyridine or non-bound pyridinium

Table 1. Selected bond lengths (Å) and angles (in degrees) for the crystallographically analyzed complexes.

Complex (E_{trz}/E)	Ir–E_{trz}	Ir–E	E–Ir–E_{trz}
1 (N_{trz}/C_{pyr})	2.042(2)	2.053(3)	76.82(11)
3 (N_{trz}/C_{pyr})	2.068(2)	2.040(3)	77.23(9)
4a (C_{trz}/N_{pyr})	2.017(2)	2.129(2)	76.08(8)
5 (C_{trz}/N_{pyr})	2.027(6)	2.124(5)	77.5(2)
6a (C_{trz}/N_{pyr})	2.013(2)	2.134(2)	76.10(9)
6b (C_{trz}/N_{pyr})	2.032(2)	2.131(2)	76.58(9)
7 (C_{trz}/C_{aryl})	2.039(3)	2.070(3)	78.44(12)
8 (C_{trz}/C_{pyr})	2.0175(14)	2.0488(14)	76.02(6)

substituents (complexes **4–7**). In the ^{13}C NMR spectrum, the iridium-bound carbon of the triazolylidene ligand experiences the largest shift-difference upon metalation (δ_C around 155 in complexes **4–8**, ca. $\Delta\delta$ ca. 30 ppm compared to the ligand precursor). The pyridylidene carbon attached to iridium was observed at slightly lower field (around 160, complexes **1, 3, 8**), while the iridium-bound carbon of the phenyl group in complexes **2** and **7** appeared at 148.8 and 144.1 ppm, respectively.

In aqueous solutions, the complexes exist as equilibria between two species. The behavior of complex **4a** is representative. Two sets of pyridyl signals were observed in D_2O, the major one featuring a low field doublet for the pyridyl H(6) proton at 8.98 ppm. All signals of the minor species are downfield shifted by 0.1–0.2 ppm (*e.g.* pyridyl H(6) proton at (δ_H 9.16). The ratio of the two species is concentration and pH dependent and shifts towards the major species at high concentrations (*e.g.* 9:1 at 20 mM solution *vs.* 7:3 at 1.7 mM), indicating an equilibrium between complex **4a** and a dicationic aquo complex. In agreement with such a notion, addition of KCl completely suppresses the presence of the minor species. Likewise, in less coordinating solvents such as CD_3OD or acetone-d_6, only one species was detected. Unambiguous evidence for the formation of such a dicationic species was obtained from irreversible abstraction of the chloride in **4a** with AgOTf in aqueous CH_2Cl_2 (Scheme 2). The NMR spectrum of the formed bis(aquo) complex **4c** matches those of the minor species. Of note in particular with regards to catalytic applications is the inertness of the complexes under strongly acidic conditions. For example, spectroscopic monitoring of the stability of complex **4a** in 1 M HCl (D_2O, pH = 0) did not indicate any changes over time (> 48 h) and no diagnostic signals due to presence of triazolium or pyridinium salts were observed. Accordingly, acidolysis of the Ir–C_{trz} bond and ensuing ligand dissociation does not occur in detectable quantities under highly acidic conditions. A similar robustness was observed for the Ir–C_{pyr} bond in complex **8**, indicating that both abnormal carbene–iridium bonds are fully acid-resistant.

All complexes except **2** and **4b** were analyzed by single crystal X-ray diffraction. The molecular structures (Figure 1) confirmed the expected connectivity patterns. The Ir–C_{trz} bond lengths are in the expected range,[55] and are consistently shorter than the corresponding Ir–N_{trz} bond lengths. Similarly, the Ir–C_{pyr} bonds

.**Figure 1**: ORTEP representations of complexes **1** (a), **4a** (b), **5** (c), **6a** (d), **7** (e), and **8** (f); all structures at 50% probability level, hydrogen atoms, non-coordinating anions, solvent molecules, and the second independent molecule in the unit cell of **5** and **7** omitted for clarity. ORTEP plots of **3** and **6b** are shown in the supporting information (Fig. S1).

are substantially shorter than the dative Ir–N$_{pyr}$ contacts. They are even slightly shorter than the Ir–C$_{aryl}$ bond in complex **7**. The ligand bite angle shows little variation, as may be expected when considering that all metalacycles in complexes **1–8** are comprised of four sp^2-hybridized carbon/nitrogen atoms and that the C–N *vs* C–C bond length difference is only minute.

Catalytic activity

The reaction of complexes **3–10** with cerium(IV) ammonium nitrate was monitored with differential digital manometry as previously described, and reaction end-points were verified with mass spectrometry.[26] Stoichiometric oxygen yields (100±4%) were observed for all new complexes (Figure 2), and in contrast to previously explored catalysts,[18] no carbon dioxide was observed during later-stages of the reaction. Close inspection of the performance of **3-10** reveals distinct differences in the catalytic activity. These differences, in conjuction with persistant NMR spectra at catalytically-relevant pH (pH = 1) and ionic strength albeit in the absence of cerium, suggest retention of the carbene-containing ligands. Further evidence of at least partial ligand retention is afforded by predictable steric and electronic effects on catalyst activity; however, the presence of a short induction period necessitates comparison of turnover frequencies at 50% conversion (Table 2).

Analogous to similar ruthenium-catalyzed water oxidation reactions,[22] steric bulk on the triazole N1 position leads to a decrease in catalytic activity (*cf* activity of **4a** *vs* **6a** and **8** *vs* **9**). Changing the ylide-carbene motif in complex **10** to a dicarbene system improved catalytic activity from 191 h^{-1} to 451 h^{-1}, suggesting the role of electronic tunability in tuning catalytic performance. Indeed, the ylide-carbene motif expresses significantly different levels of activity and may possess an entirely different reaction mechanism. The *C-C* chelate appears to effect greater activity than an *N-C* chelate from a comparison of complexes **4a** and **8**. And, as illustrated by the poor performance of complex **3**, increasing the ligand donor properties from triazole *N*-coordination to triazolylidene *C*-bonding (c.f. **8**) is beneficial and leads to greater activity.

In contrast to reports suggesting the formation of a heterogeneous species implicated as an active intermediate in the water oxidation reaction,[31–33] exploratory reactions yielded no

particles visible to the naked eye and prompted further study. While later experiments employing dynamic light scattering were able to observe the formation of dioxygen bubbles, no scattering attributable to iridium nanoparticles was observed from any reaction of complexes **4a/4c** or **8** at least to the limits of detection (ca. 1-2 nm, See ESI for DLS results).

Mechanistic details

Definitively interpreting the reaction progress into discrete mechanistic steps is complicated by numerous factors: the initial preequilibrium due to solvolysis, disproportionation between catalytic intermediates and various cerium(III)/cerium(IV) species[56–58], the effects of ionic strength, and the potential interactions of any supporting and non-innocent ions with reaction intermediates. There is also a high likelihood that reactions driven by the ostensibly single-electron oxidant cerium would have significantly different electron transfer mechanisms than periodate driven reactions which would be different still from electrode driven reactions[59–61] and render direct comparisons between methods inconclusive at best. Moreover, any investigation involving ex situ analysis, for example electron microscopy following solvent evaporation, may lead to potentially misleading conclusions as the sample preparation will inherently affect the constitution of the observed species. We therefore set out to analyze reactions with non-invasive "*in operando*" techniques.[62]

Despite the reaction complexity, important information can be garnered from in-depth kinetic investigations. Three different types of experiments conducted on the most active species, **4a**, provided a significant quantity of relevant information: varying the catalyst concentration (Figure 3), varying the cerium concentration (Figure 4), and step-wise addition of cerium to

Table 2. Turnover frequencies at 50% conversion, TOF$_{50}$
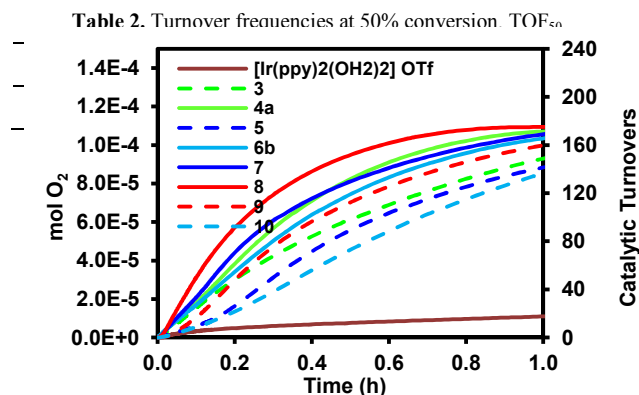
Figure 2: Catalytic activity of complexes **3–10** and [Ir(ppy)$_2$(OH$_2$)$_2$]OTf at 0.5±0.05 mM catalyst and 0.45 M cerium(IV). (1 mL total volume). All solutions produced oxygen consistent with the stoichiometric limit of added CAN.
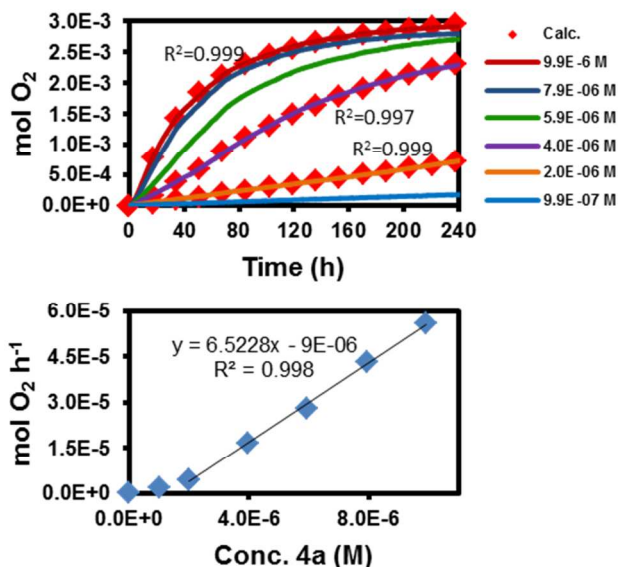
Figure 3 Top: O$_2$ formation for complex **4a** at concentrations ranging up to 10 μM following addition to 20 mL aqueous cerium ammonium nitrate solutions (0.835 M). The dotted trace describes a least squares fit employing the integrated rate law described in Scheme 3. **Bottom**: Plot of maximum rate of O$_2$ formation from above illustrating concentration-dependent mechanism.

catalyst solutions (Figure 5). While an impressive number of total turnovers (mole O_2 per mole precursor) in excess of 30,000 were common in extended oxidation experiments,[60,63] the combined results of these three experiments reveals nuanced patterns that describe the underlying catalyst behaviour.

Varying the concentration of **4a** from 1 μM to 10 μM with a large excess of cerium(IV) suggests the major reaction path varies based on the concentration of **4a**, in agreement with papers describing the activity of dinuclear iridium complexes[63,64]. At low catalyst concentrations (≤ 2 μM), oxygen evolution was found to be linear with respect to time while at higher concentrations of **4a** (> 2 μM) the reaction appears to be limited by higher order steps (Figure 3). In particular, note the sigmoidal response of the 4 μM trace which conclusively eliminates the possibility of a simple single or double exponential fit. Further support of a series of sequential first order reactions at higher concentrations of catalyst is provided by the application of factor analysis to the UV-visible response of catalyst solutions.

At higher precatalyst **4a** concentrations, support for a series of sequential first order reactions leading to oxygen evolution is first suggested by the acceleration of the rate of oxygen production at 4μM. More stringent support is afforded by applying the integral method[65] to the oxygen evolution traces. Accordingly, a semi-log plot of reaction progress vs. time will be linear when the dominant reaction order is one while a linear scale will produce a straight line when the dominant reaction order is two. Examining first and second-order linearized plots of the oxygen evolution traces from experiments similar to those described in Figure 3 reveals two regions with differing reaction order (See Figure S2 for an example). The initial activity sums the constituent reactions to an overall order of two then gradually gives way to slower, overall first-order behaviour.

The catalytic species evolving into dioxygen and a dioxygen-deficient species requires a preceding (pseudo)first order reaction. Neglecting the contributions of cerium dependence, the two (pseudo)first order reactions resulting in oxygen formation can be modelled as in Scheme 3. Accordingly, the value C_{O_2} represents the integrated quantity of oxygen, the value of $C°_A$ represents the total quantity of oxygen-evolving precursor formed over the entire course of the reaction. Interestingly, the integrated quantity of A was determined to be one half of the number of equivalents of cerium(IV). Since the quantity of oxygen produced is stoichiometrically determined by the quantity of cerium added this suggests the initial species or resting state is a 2 electron intermediate analogous to the putative cerium-coordinated species described in similar works employing ruthenium and iron.[67-69]

Scheme 3

$$A \xrightarrow{k_1} B \xrightarrow{k_2} C + O_2$$
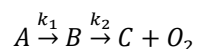
$$C_{O_2} = C_A° \left(1 - \frac{k_2 \exp(-k_1 t) - k_1 \exp(-k_2 t)}{k_2 - k_1}\right)$$

As seen by the dotted traces in Figure 3, there is excellent

agreement between least-squares fitting of the integrated rate law from Scheme 3 and the experimentally observed oxygen evolution data from all three regions of catalytic activity (overall second order at high catalyst concentration, pseudo-sigmoidal behavior due to consecutive reactions, and overall first order at low catalyst concentrations)

In this "high" concentration range, the maximum rate of oxygen evolution for **4a** was found to be linearly correlated to catalyst concentration with deviation from linearity at concentrations below 2 μM suggesting a fundamental change in mechanism or rate limiting step outside of this range (Figure 3, bottom). Additionally, a log-log plot of rate vs. catalyst concentration indicates the presence of a mixed order reaction (Slope of 1.5; Figure S3d).

The effect of varying the cerium concentration from 3 mM to 0.865 M while holding the concentration of **4a** at 8.6 μM is shown in Figure 4. Cerium solutions were buffered in 1N HNO_3 for four primary reasons: i) to prevent the thermodynamic decay of cerium(IV) at high pH values; ii) to avoid reaction complexity by limiting the speciation of ions present; iii) to take advantage of faster reaction kinetics;[66] and iv) to preclude the precipitation of cerium(III) species. These conditions may also increase the solubility or decrease the propensity for aggregation of iridium
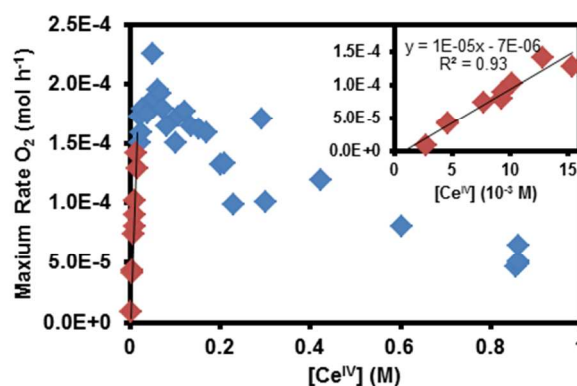
Figure 4: Variation of maximum O_2 rate due to changing cerium(IV) concentration at 8.6 μM **4a** in 1N HNO_3. Inset: Expanded scale of 0 mM to 15 mM illustrating linear trend in maximum rate at low cerium(IV) concentrations.

species and an important caveat comes from the wide variation in ionic strength across this concentration.

Under these conditions the maximum rate of oxygen production occurs at 50 mM cerium(IV) with 0.18 mmol O_2 h^{-1} (TOF 20.9 h^{-1}). Prior to this maximum, between 0-20mM cerium(IV) or roughly 300-2400 cerium(IV) equivalents, the rate of maximum oxygen evolution increases linearly suggesting a first order dependence on cerium(IV). A gradual decrease in the maximum rate of oxygen evolution is observed at concentrations greater than 100 mM cerium(IV), likely the result of the significantly increased ionic strength or the aggregation of cerium(IV) into dimeric species.[58] This initial first order behaviour and concentration-dependent inhibition is consistent with mechanisms involving either inner sphere electron transfer or the fast decay of a M-O-O-Ce species as described in similar ruthenium and iron water oxidation studies.[67-69]

As observed previously with related Ir(Cp*) complexes,[70] addition of CAN induced a colour change of the initial yellow

solution to blue within seconds. While the formation of a blue mixture or a blue layer[70] has periodically been attributed to IrO_x formation due to the oxide's general tendency to absorb broadly around 580 nm[28,31] similar color changes have previously been noted in high-valent iridium aquo complexes[71] and for an iridium μ-oxo dimer.[72]

As UV-vis may provide insight into the catalyst speciation, early stages of the reaction of **4a** were investigated by sequential additions of 20 equivalents of cerium(IV) with concurrent UV/Vis and manometric measurements (Figures 5 and 6). When a single addition of 20 equivalents of CAN was added to a 0.5 mM solution of **4a** no measurable oxygen production was observed (Figure 5) though a rapid color change from yellow to blue and back occurs over the course of 15 minutes (Figure 6, top left). After 8 hours, a second aliquot of 20 equivalents of CAN was added and 8 hours later another addition of 20 equivalents. This process was repeated for a total of 8 steps or 160 total equivalents of CAN over 64 hours. A sub-stoichiometric quantity of oxygen was produced during the second through fourth additions with the deviation from stoichiometric predictions decreasing on each subsequent addition. Approximately 30 equivalents of cerium in total are unaccounted for by manometry.

No carbon dioxide was observed via headspace mass spectrometry even when the experiment was repeated with double the concentration of catalyst. The gas analyser employed is ostensibly sensitive into the ppm range; but, more conservatively if even one mole of CO_2 was produced per mole of catalyst it would occupy 1-2%mol of the overall headspace i.e. well within the limits of detection. One feasible contribution to the cerium discrepancy investigated was oxidation of the initial chloride ligand to perchlorate either by cerium or oxidized catalyst via $ClO_4^- + 4\ H_2O + 8e^- \rightarrow Cl^- + 8OH^-$ at 0.56 V. As a control, the experiment was repeated with an aquo complex, **4c**, yielding no significant differences from the chloride analogue **4a** (Figure 5, blue overlay).

Progressively examining each oxygen evolution trace through the method of first and second-order linearizations[65] yields the same sequential first order behavior observed from analysis of Figure 3. Least squares fitting of the integrated rate equation described in Scheme 3 to the final four oxygen evolution steps yield first order rate constants, k_1 and k_2, of ca. 40 hr^{-1} and 13 hr^{-1}
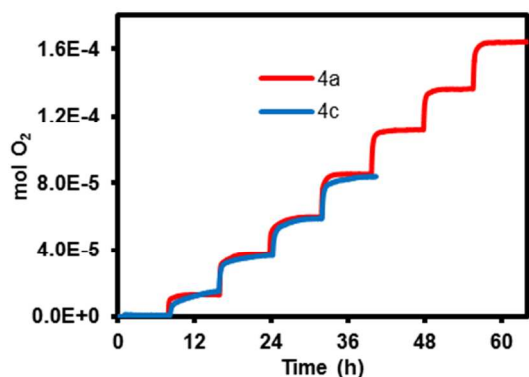
Figure 5: Stepped oxygen production following addition of 20 equivalents cerium(IV) to 0.5 mM **4a** in 1N HNO_3 with an 8 hour interval between additions overlaid with the same experiment with **4c**. No oxygen production occurs for the first thirty equivalents of cerium(IV) with stoichiometric oxygen production occurring after the third addition.

respectively (Figure S4).

While the initial rates of all oxygen-producing steps were identical, the first four steps were poorly fit by the sequential first order model and not assessed as such. The purported active species of oxidant, Ce(IV)OH, exists in an equilibrium with a relatively less active μ-oxo dimer. This deviation is likely caused by a combination of the concentration-dependent equilibrium of the active oxidant species, Ce(IV)OH, and the necessity of oxidative transformations to the catalytically active iridium species. Indeed, a paramagnetic cerium ion coupled to the iridium catalyst would further explain the decrease in intensity and broadening of NMR signals following addition of CAN to catalyst described later in this manuscript. EPR spectroscopy at numerous concentrations of CAN and catalyst was unable to identify species besides the broad absorption of cerium(III).

Long-term catalyst deactivation was assessed by plotting the rate of oxygen evolution vs. the quantity of oxygen evolved for the final four steps. These plots yielded overlapping traces demonstrating the absence of catalyst deactivation[73] following the initial induction period; the active catalyst species in the experiments with a gross excess of cerium are therefore likely the same species present after the fourth addition of cerium in the stepwise experiments.
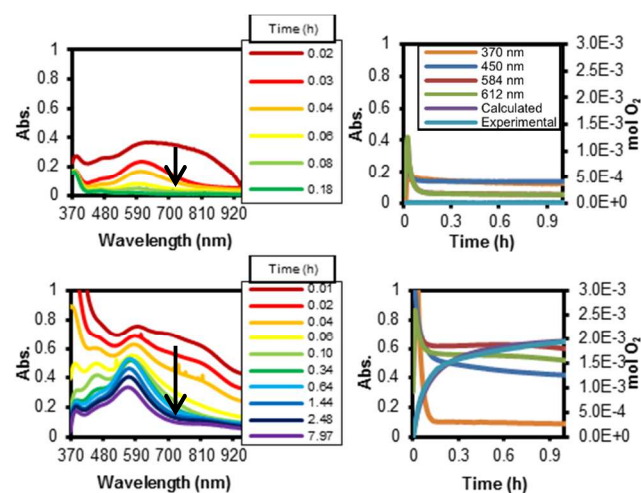
Figure 6 Left: Chronological spectra from the first (top) and fourth (bottom) addition of 20 equivalents cerium(IV). Spectra are indexed in hours relative to the preceding cerium(IV) addition. **Right**: Absorption traces with experimental and fitted (Scheme 4) oxygen evolution traces in purple and light blue for the first (top) and fourth (bottom) addition of 20 equivalents of cerium(IV).

The UV-vis spectra versus time data from the final four stepwise additions to the experiment described in Figure 5 were assembled into matrices of [time, wavelength] (Y) which was then analysed with singular value decomposition. Both the subjective method of a semi-log plot of the singular values and the minima in the factor indicator function[74] were used to assess the rank of these matrices suggesting the presence of five iridium-containing species. The reduced matrix ($\overline{Y}$), reconstructed with the significant singular values, was plotted with the residual signal to confirm the absence of additional species within the limits of detection (Figure S5). Normalized concentration profiles (C) and molar absorptivities (A) of the individual species were obtained from this reconstructed matrix using resolving factor
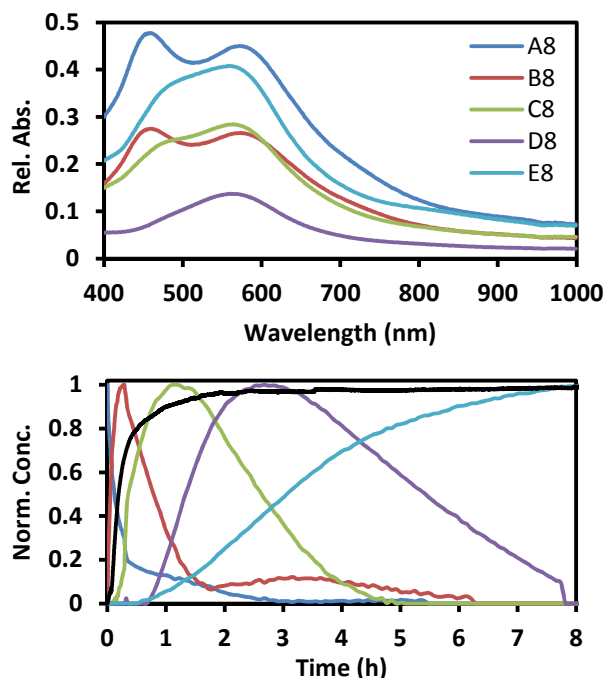
Figure 7 Top: Individual component spectra of species A through E from the eighth addition. **Bottom:** Normalized concentration of species A through E and corresponding oxygen evolution trace (black line) from the eighth addition of cerium(IV).

analysis.[75,76] Briefly, evolving factor analysis was used to provide an initial guess for a Levenberg-Marquardt minimisation of the residuals of the equation $R = \overline{Y} - CA = \overline{Y} - (\overline{U}T) \times (T^{-1} \overline{S} \overline{V})$ subject to the constraints that the matrices C and A are both non-negative and the concentration profiles are unimodal above a threshold of 0.2 normalized concentration.

The individual iridium-containing component spectra (Figure 7, Top) did not correspond with solvent-corrected DFT calculations of UV-vis spectra belonging to proposed mononuclear species of **4a** lending further credence to the notion of a rutile dinuclear iridium species.[72] Modelling the numerous potential dinuclear species is complicated by long geometry optimizations and produces only modest agreement between the observed individual component spectra (Figure S11). A plausible discussion of kinetics conjectures similar steps to the related ruthenium or iron water oxidation catalysts[67,68] via a dinuclear Ir(III,III) to Ir(V,V) or Ir(IV,V) with peroxo-coupled cerium species but currently lacks inarguable evidence besides the suggestion of aquo Ir(III,III) and peroxo-containing species. However, calculations do suggest the participation of the mononuclear iridium(V) species in the role of pre-catalyst activation as the hapticity of the Cp* moetiy is predicted to change via solvolysis and oxidation of **4c**. (See Supporting Information for complete set of calculated compounds and comparison of observed and calculated spectra)

The normalized concentration profiles resulting from factor analysis (Figure 7, Bottom) are highly supportive of the sequential first order behaviour suggested from the first and second order linearizations and the least squares fitting presented

above. Species A and B from the figure correspond to the proposed pathway in Scheme 3 while species C corresponds to the dioxygen-deficient intermediate. The maximum rate of oxygen production occurs, with reasonable agreement, at the maximum concentration of species **B**, putatively the oxygen-releasing intermediate. Species D and E would then represent a solvation and preparatory intermediates that would then be triggered by further addition of cerium(IV).

In contrast to Grotjahn et al.[31] no precipitate was observed at any point. Dynamic light scattering measurements of a 5 mM solution of **4a** in 1N HNO_3 following addition of 20 equivalents of CAN produced variable scattering intensities over time. Scattering indicating particle sizes as large as 1000 nm were observed by the fourth addition of 20 equivalents; however application of a slight vacuum to the solution causes a decrease in the observed size. Additionally, after 40 hours at atmospheric pressure, particle sizes returned to the baseline measurements of typical cerium(IV)/cerium(III) solutions (Figures S8-13).[77] These observations strongly suggest that any scattering intensity observed via DLS is derived from the nucleation of dioxygen and not from metal-containing nanoparticulates or nanoclusters.

In an attempt to further elucidate the reaction mechanism, NMR measurements under identical conditions indicated that **4a** undergoes rapid solvolysis when dissolved in water to produce a mixture of **4a** and **4c** with a chloride counter ion in a 4:1 ratio. Following addition of 10 equiv. cerium(IV) to the 1 mM NMR sample, integrals of both **4a** and **4c** decrease and the ratio of **4a**:**4c** decreases from 4:1 to 2:1. Repeating the experiment with the addition of 2 equiv cerium(IV) establishes a 3:1 ratio of **4a**:**4c**. The integrals and ratios remained constant over several days, yet all signals disappeared upon addition of a second 10 equiv cerium(IV), indicating the formation of a paramagnetic species. Addition of 20 equiv CAN to a fresh solution of **4a** buffered in 1 N HNO_3 yielded identical results. NMR signals at 8.25 ppm lends support to the formation of formaldehyde which is in agreement with proposed oxidation mechanisms of carbene wingtip methyl groups.[30,78] The Cp* methyl signal is noticeably downfield shifted from the original spectra of **4a** following addition of CAN and broad signals of the chelating carbene are clearly present (Figures S15-16).

The reproducible and well-behaved reaction kinetics, negative results from dynamic light scattering experiments, a lack of carbon dioxide from headspace gases, and significantly faster rate of reaction compared to IrO_2 all reinforce the molecular nature of active species derived from **4a**. Additionally, modifications to the ligand scaffold have noticeable and predictable effects on the reaction kinetics. While it is difficult, with complete certainty, to eliminate the presence of a heterogeneous species active towards water oxidation, especially under catalytically relevant conditions with very low catalyst loading, this work shows that the most competent catalytically active species under the conditions applied here is likely a molecular species which catalyzes water oxidation in two sequential first-order molecular reaction steps.

Mesoionic triazolylidenes may be particularly suitable as ligands for the ensuing redox processes. Their strongly mesoionic character is capable of stabilizing various redox states and may give rise to proton-coupled electron transfer (PCET) from a putative iridium hydroxide intermediate to the triazolylidene

ligand (Scheme 4). Previous results with related abnormal carbene ligands demonstrated that the mesoionic carbene ligand is involved in hydrogen exchange reactions and in metal-catalyzed E–H bond breaking processes (Scheme 4).[79,80]
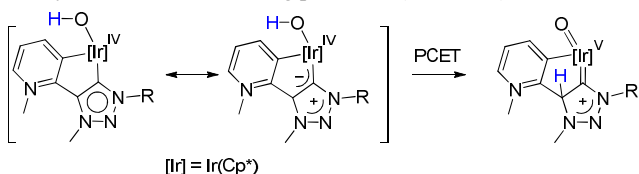
Scheme 4

Conclusions

A variety of iridium complexes comprising mesoionic carbene ligands were synthesized and found to serve as competent precatalysts for the oxidation of water. Turnovers above 30,000 were recorded with TOFs exceeding 450 h^{-1} for the most active catalytic system. This turnover number is limited by the availability of sacrificial oxidant and not by the robustness of the catalyst, which suggests these types of catalysts may be suitable for continuous water oxidation processes. Mechanistic investigations, especially under stoichiometric or near stoichiometric conditions, strongly support a tunable molecular species as the catalytic entity. Additionally, dynamic light scattering measurements support the absence of light scattering particles not incipiently present in cerium solutions. While it is not possible to definitively exclude multiple active catalytic species of differing composition, this work together with mechanistic studies of similar dinuclear iridium complexes[63,64] strongly supports the presence of a homogeneous, tunable, and long-lived iridium water oxidation catalyst. Future work is directed towards developing an intimate understanding of the catalytic mechanism under various conditions.

Experimental Section

General

All syntheses of the iridium complexes were carried out under an inert atmosphere of N$_2$ using Schlenk technique and dry solvents. Purifications, including column chromatography, were performed in air using commercial solvents. All ^{1}H and ^{13}C{^{1}H} NMR spectra were recorded at room temperature on Bruker or Varian spectrometers and chemical shifts were referenced to SiMe$_4$ for organic solvents and to the temperature-corrected residual DHO peak in aqueous experiments (δ in ppm, J in Hz). The ligand precursors **L4** and **L6**,[22] the precursor compounds 2-(1-methyl-1H-1,2,3-triazol-4-yl)pyridine,[22] 2-(1-phenyl-1H-1,2,3-triazol-4-yl)pyridine,[22] 5-methyl-1-phenyl-1H-1,2,3-triazole,[81] [Cp*IrCl$_2$]$_2$,[82] and the complexes **9** and **10**[26] were prepared according to literature procedures. All other reagents were purchased from commercial sources and were used as received.

L1: A suspension of 2-(1-phenyl-1H-1,2,3-triazol-4-yl)pyridine (460 mg, 2.07 mmol) and MeOTf (0.41 mg, 2.48 mmol) in CH$_2$Cl$_2$ (5 mL) was stirred at 0° C for 30 minutes. Excess Et$_2$O was added and the supernatant was removed by decantation. The tan oil was repeatedly washed with Et$_2$O. NMR spectroscopy of the crude sample indicated non-selective methylation and the presence of two compounds **L1** and **L6** in approximate 2:1 ratio.

They were separated by preparative TLC using SiO$_2$ plates and MeCN/CH$_2$Cl$_2$ (1:3 v/v) as eluent. **L6** eluted first;[22] the second band contained **L1** and was extracted from SiO$_2$ by stirring in MeOH and subsequent filtration. The volatiles were removed under reduced pressure and the residue was dissolved in CH$_2$Cl$_2$ and filtered again. The solvent was evaporated and pentane was added. The precipitate was collected and dried in vacuo, thus giving **L1** as a white solid (150 mg, 20%). ^{1}H NMR (CD$_3$CN, 400 MHz): 9.09 (s, 1H, H$_{trz}$), 8.79 (d, $^3J_{HH}$ = 6.2 Hz, 1H, H$_{py}$), 8.58 (t, $^3J_{HH}$ = 8.0 Hz, 1H, H$_{py}$), 8.51 (d, $^3J_{HH}$ = 8.0 Hz, 1H, H$_{py}$), 8.0 (dd, $^3J_{HH}$ = 8.0 Hz, $^3J_{HH}$ = 6.2 Hz, 1H, H$_{py}$), 7.97 (d, $^3J_{HH}$ = 7.4 Hz, 2H, H$_{Ph}$), 7.68 (d, $^3J_{HH}$ = 7.4 Hz, 2H, H$_{Ph}$), 7.59 (t, $^3J_{HH}$ = 7.4 Hz, 1H, H$_{Ph}$), 4.53 (s, 3H, N$_{trz}$–CH$_3$). ^{13}C{^{1}H} NMR (CDCl$_3$, 100 MHz): 147.4, 146.3, 145.8, 139.5, 136.5, 130.3, 130.1, 129.2, 127.1, 126.7 (C$_{trz}$–H), 121.3, 48.6 (N$_{trz}$–CH$_3$). Anal. calcd. for C$_{15}$H$_{13}$F$_3$N$_4$O$_3$S (386.35): C, 46.63; H, 3.39; N, 14.50 %. Found: C, 46.58; H, 3.31; N, 14.39 %.

L3: The procedure was identical to that described for **L1** starting from 2-(1-methyl-1H-1,2,3-triazol-4-yl)pyridine (400 mg, 2.50 mmol) and MeOTf (450 mg, 2.75 mmol), thus giving a crude mixture of **L3** and **L4** in approximate 1:1 ratio. Preparative TLC purification yielded **L3** as the second fraction, which was isolated as described for **L1**, yielding the title product as a white solid (195 mg, 24%). ^{1}H NMR (CD$_3$CN, 500 MHz): δ 8.74 (d, $^3J_{HH}$ = 6.2 Hz, 1H, H$_{py}$), 8.58 (s, 1H, H$_{trz}$), 8.54 (t, $^3J_{HH}$ = 7.8 Hz, 1H, H$_{py}$), 8.43 (d, $^3J_{HH}$ = 7.8 Hz, 1H, H$_{py}$), 7.97 (dd, $^3J_{HH}$ = 7.8 Hz, $^3J_{HH}$ = 6.2 Hz, 1H, H$_{py}$), 4.46 (s, 3H, N$_{py}$–CH$_3$), 4.24 (s, 3H, N$_{trz}$–CH$_3$). ^{13}C{^{1}H} NMR (CDCl$_3$, 125 MHz): δ 147.0, 145.6, 138.6, 138.4, 129.2 (C$_{trz}$–H), 128.8, 126.6, 48.4 (N$_{py}$–CH$_3$), 37.1 (N$_{trz}$–CH$_3$). Anal. calcd. for C$_{10}$H$_{11}$F$_3$N$_4$O$_3$S (324.28): C, 37.04; H, 3.42; N, 17.28 %. Found: C, 37.02; H, 3.33; N, 16.97 %.

L5: A mixture of 5-methyl-1-phenyl-1H-1,2,3-triazole (200 mg, 1.26 mmol) and 2-bromopyridine (198 mg, 1.26 mmol) was heated in a sealed vial at 160 °C for 36 h. The resulting brown solid was dissolved in H$_2$O (50 mL) and excess NaPF$_6$ was added. An immediate precipitation was observed. The mixture was stirred for 1 h and then filtered. The residue was washed with copious amounts of H$_2$O and subsequently with Et$_2$O and dried in vacuo to give **L5** as a white solid (250 mg, 52%). Recrystallization from MeCN/Et$_2$O yielded analytically pure material. ^{1}H NMR (CD$_3$CN, 500 MHz): δ 9.16 (s, 1H, H$_{trz}$), 8.75 (d, $^3J_{HH}$ = 4.7 Hz, 1H, H$_{py}$), 8.24 (td, $^3J_{HH}$ = 7.6 Hz, $^4J_{HH}$ = 1.6 Hz, 1H, H$_{py}$), 8.19 (d, $^3J_{HH}$ = 7.6 Hz, 1H, H$_{py}$), 7.88–7.77 (m, 6H, H$_{py}$+H$_{Ph}$), 2.61 (s, 3H, C$_{trz}$–CH$_3$). ^{13}C{^{1}H} NMR (CD$_3$CN, 125 MHz): δ 149.9, 146.9, 142.8, 141.2, 133.8, 132.8, 130.6, 127.8, 125.76, 125.75, 125.69, 125.67 (C$_{trz}$–H), 115.2, 9.6 (CH$_3$). Anal. calcd. for C$_{14}$H$_{13}$F$_6$N$_4$P (382.24): C, 43.99; H, 3.43; N, 14.66 %. Found: C, 44.00; H, 3.37; N, 14.46 %.

L7: A suspension of 2-(1-phenyl-1H-1,2,3-triazol-4-yl)pyridine (370 mg, 1.67 mmol) and MeOTf (1.37 mg, 8.3 mmol) in dry CH$_2$Cl$_2$ (8 mL) was stirred at 45 °C for 12 h. The formed precipitate was collected by filtration, washed with CH$_2$Cl$_2$ and then with Et$_2$O and dried in vacuo to afford **L7** as a white solid (606 mg, 66%). ^{1}H NMR (500 MHz, CD$_3$CN): 9.40 (s, 1H, H$_{trz}$), 9.10 (d, $^3J_{HH}$ = 6.1 Hz, 1H, H$_{py}$), 8.79 (td, $^3J_{HH}$ = 7.9 Hz, $^4J_{HH}$ = 0.8 Hz, 1H, H$_{py}$), 8.39 (dd, $^3J_{HH}$ = 7.9 Hz, $^4J_{HH}$ = 1.3 Hz, 1H, H$_{py}$), 8.35 (ddd, $^3J_{HH}$ = 7.9 Hz, $^3J_{HH}$ = 6.1 Hz, $^4J_{HH}$ = 1.3 Hz, 1H, H$_{py}$), 8.01–7.97 (m, 2H, H$_{Ph}$), 7.81–7.75 (m, 3H, H$_{Ph}$), 4.37 (s,

3H, N_{trz}–CH_3), 4.36 (s, 3H, N_{py}–CH_3). $^{13}C\{^1H\}$ NMR (CD$_3$CN, 125 MHz): δ149.8, 147.3, 136.7, 134.9, 133.6, 132.8, 131.6, 131.4 (C_{trz}–H), 130.8, 122.4, 48.3 (N_{py}–CH_3), 40.2 (N_{trz}–CH_3). Anal. calcd. for $C_{17}H_{16}F_6N_4O_6S_2$ (550.45): C, 37.09; H, 2.93; N, 10.18 %. Found: C, 36.83; H, 2.74; N, 10.48 %.

L8: Compound **L8** was prepared analogously to **L7** starting from 2-(1-methyl-1H-1,2,3-triazol-4-yl)pyridine (400 mg, 2.50 mmol) and MeOTf (1.64 g, 10 mmol) and was obtained as a white solid (1.10 g, 90%). ^1H NMR (DMSO-d$_6$, 300 MHz): δ 9.37 (d, $^3J_{HH}$ = 5.8 Hz, 1H, H_{py}), 9.23 (s, 1H, H_{trz}), 8.86 (td, $^3J_{HH}$ = 7.9 Hz, $^4J_{HH}$ = 0.8 Hz, 1H, H_{py}), 8.48–8.42 (m, 2H, H_{py}), 4.46, 4.27 (2 × s, 3H, N_{trz}–CH_3), 4.26 (s, 3H, N_{py}–CH_3). $^{13}C\{^1H\}$ NMR (CD$_3$CN, 125 MHz): δ 149.6, 146.9, 17.6, 134.5 (C_{trz}–H), 132.7, 132.1, 130.8, 47.9 (N_{py}–CH_3), 40.9, 39.6 (2 × N_{trz}–CH_3). Anal. calcd. for $C_{12}H_{14}F_6N_4O_6S_2$ (488.38): C, 29.51; H, 2.89; N, 11.47 %. Found: C, 30.22; H, 3.01; N, 11.29 %.

Complexes 1 and 2: A mixture of **L1** (92 mg, 0.25 mmol), AgOAc (63 mg, 0.37 mmol) and [Cp*IrCl$_2$]$_2$ (100 mg, 0.13 mmol) in MeOH (10 mL) was refluxed for 24 h and then filtered through Celite. The filtrate was concentrated to ca. 2 mL, which induced crystallization of the orange complex **1** (50 mg, 20%). The mother liquor was evaporated and the residue washed with copious amounts of CHCl$_3$ until the washing was essentially colorless, thus leaving complex **2** as a yellow solid (30 mg, 12%). Analytical data for **1**: ^1H NMR (CD$_3$CN, 400 MHz): δ 9.06 (s, 1H, H_{trz}), 8.71 (d, $^3J_{HH}$ = 7.2 Hz, 1H, H_{py}), 8.31 (d, $^3J_{HH}$ = 6.1 Hz, 1H, H_{py}), 8.03 (d, $^3J_{HH}$ = 7.7 Hz, 2H, H_{Ph}), 7.75–7.66 (m, 3H, H_{Ph}), 7.59 (dd, $^3J_{HH}$ = 7.2 Hz, $^3J_{HH}$ = 6.1 Hz, 1H, H_{py}), 4.46 (s, 3H, N–CH_3), 1.80 (s, 15H, C_{Cp}–CH_3). $^{13}C\{^1H\}$ NMR (CD$_3$CN, 100 MHz): δ 162.0 (C_{py}–Ir), 152.0, 150.4, 147.4, 139.2, 136.4 130.8, 130.5, 125.7, 124.8 (C_{trz}–H), 121.3, 90.9 (C_{Cp}), 47.9 (N–CH_3), 8.5 (C_{Cp}–CH_3). Anal. calcd. for $C_{25}H_{27}ClF_3IrN_4O_3S$ (478.24): C, 40.13; H, 3.64; N, 7.49 %. Found: C, 39.59; H, 3.52; N, 7.32 %. Single crystals of **1** that were suitable for X-ray diffraction were obtained from the corresponding tetraphenylborate salt. This salt was obtained by adding NaBPh$_4$ (20.5 mg, 0.06 mmol) to a solution of **1** (10 mg, 0.01 mmol) in MeOH (2 mL). After stirring for 30 minutes, the yellow precipitate was collected, washed twice with MeOH and finally with Et$_2$O and then dried in vacuo. The ^1H NMR spectrum does not show any significant change except for the new resonances at δ 7.30, 7.01 and 6.86 due to the BPh$_4^-$ anion. The ^{19}F NMR spectrum is empty and does not show any signal in the range expected for the triflate anion.

Analytical data for **2**: ^1H NMR (CD$_3$CN, 500 MHz): δ 9.17 (s, 1H, H_{trz}), 8.79 (d, $^3J_{HH}$ = 6.1 Hz, 1H, H_{py}), 8.62 (t, $^3J_{HH}$ = 8.0 Hz, 1H, H_{py}), 8.50 (dd, $^3J_{HH}$ = 8.0 Hz, $^4J_{HH}$ = 1.4 Hz, 1H, H_{py}), 8.05 (ddd, $^3J_{HH}$ = 8.0 Hz, $^3J_{HH}$ = 6.2 Hz, $^4J_{HH}$ = 1.4 Hz, 1H, H_{py}), 7.90, 7.79 (2 × dd, $^3J_{HH}$ = 7.4 Hz, $^4J_{HH}$ = 1.3 Hz, 1H, H_{Ph}), 7.32 7.25 (2 × td, $^3J_{HH}$ = 7.4 Hz, $^4J_{HH}$ = 1.3 Hz, 1H, H_{Ph}), 4.56 (s, 3H, N–CH_3), 1.82 (s, 15H, C_{Cp}–CH_3). $^{13}C\{^1H\}$ NMR (CD$_3$CN, 125 MHz): δ 148.8 (C_{Ph}–Ir), 147.6, 145.9, 140.0, 139.5, 137.2, 133.9, 129.5, 129.3, 127.4, 124.1 (C_{trz}–H), 123.5, 113.7, 90.4 (C_{Cp}), 48.8 (N–CH_3), 8.4 (C_{Cp}–CH_3). Anal. calcd. for $C_{25}H_{27}ClF_3IrN_4O_3S$ (478.24): C, 40.13; H, 3.64; N, 7.49 %.

Complex 3: Compound **L3** (120 mg, 0.37 mmol), AgOAc (124 mg, 0.74 mmol) and [Cp*IrCl$_2$]$_2$ (147 mg, 0.18 mmol) was refluxed in dry MeOH (12 mL) for 18 h. The reaction mixture

was filtered through Celite and concentrated to ca. 4 mL. Crystallization was induced upon standing at room temperature and afforded pure **3** as an orange solid (60 mg, 35%). ^1H NMR (CD$_3$CN, 300 MHz): δ 8.65 (dd, $^3J_{HH}$ = 7.7 Hz, $^4J_{HH}$ = 0.7 Hz, 1H, H_{py}), 8.52 (s, H_{trz}, 1H), 8.24 (dd, $^3J_{HH}$ = 5.9 Hz, $^4J_{HH}$ = 0.7 Hz, 1H, H_{py}), 7.53 (dd, $^3J_{HH}$ = 7.7 Hz, $^3J_{HH}$ = 5.9 Hz, 1H, H_{py}), 4.33 (s, 3H, N_{py}–CH_3), 4.29 (s, 3H, N_{trz}–CH_3), 1.74 (s, 15H, C_{Cp}–CH_3). $^{13}C\{^1H\}$ NMR (CD$_3$CN, 125 MHz): δ 161.5 (C_{py}–Ir), 151.6, 150.6, 146.2, 138.5, 127.62 (C_{trz}–H), 125.1, 90.3 (C_{Cp}), 47.4 (N_{py}–CH_3), 38.6 (N_{trz}–CH_3), 8.1 (C_{Cp}–CH_3). Anal. calcd. for $C_{20}H_{25}ClF_3IrN_4O_3S$ (686.17): C, 35.01; H, 3.67; N, 8.17 %. Found: C, 34.88; H, 3.49; N, 7.99 %.

Complex 4a: A suspension of **L4** (70 mg, 0.216 mmol), Ag$_2$O (50 mg, 0.216 mmol) and [Cp*IrCl$_2$]$_2$ (86 mg, 0.108 mmol) in CH$_2$Cl$_2$ (15 mL) was stirred for 18 h. After filtration through Celite, the volume was reduced to ca. 1 mL and excess Et$_2$O was added. The resulting precipitate was filtered off and purified by column chromatography (SiO$_2$; CH$_2$Cl$_2$/MeCN). The yellow fraction was collected, evaporated, and dried in vacuo to give complex **4a** as a yellow solid (80 mg, 54%). ^1H NMR (CD$_3$CN, 300 MHz): δ 8.74 (d, $^3J_{HH}$ = 5.7 Hz, 1H, H_{py}), 8.10–8.02 (m, 2H, H_{py}), 7.49–7.41 (m, 1H, H_{py}), 4.51, 4.30 (2 × s, 3H, N_{trz}–CH_3), 1.73 (s, 15H, C_{Cp}–CH_3). $^{13}C\{^1H\}$ NMR (CD$_3$CN, 125 MHz): δ 157.5 (C_{trz}–Ir), 153.9, 148.9, 147.9, 139.9, 126.4, 121.4, 91.1 (C_{Cp}), 39.9, 38.9 (2 × N_{trz}–CH_3), 8.8 (C_{Cp}–CH_3). Anal. calcd. for $C_{20}H_{25}ClF_3IrN_4O_3S$ (686.17): C, 35.01; H, 3.67; N, 8.17 %. Found: C, 34.98; H, 3.68; N, 8.06 %.

Complex 4b: A mixture of **4a** (100 mg, 0.15 mmol) and AgOTf (56 mg, 0.218 mmol) was refluxed in MeCN (10 mL) for 24 h. It was filtered through Celite and the filtrate was evaporated to dryness, washed with CHCl$_3$ (4 × 1 mL), and dried in vacuo, thus affording complex **4b** as a yellowish solid (78 mg, 78%). ^1H NMR (CD$_3$CN, 300 MHz): δ 9.20 (d, $^3J_{HH}$ = 5.6 Hz, 1H, H_{py}), 8.27–8.14 (m, 2H, H_{py}), 7.69 (ddd, $^3J_{HH}$ = 7.4 Hz, $^3J_{HH}$ = 5.6 Hz, $^4J_{HH}$ = 2.0 Hz, H_{py}, 1H), 4.59, 4.53 (2 × s, 3H, N_{trz}–CH_3), 1.70 (s, 15H, C_{Cp}–CH_3). $^{13}C\{^1H\}$ NMR (CD$_3$CN, 125 MHz): δ 154.6 (C_{trz}–Ir), 151.1, 149.4, 149.3, 141.5, 127.3, 122.3, 93.7 (C_{Cp}), 40.5, 39.1 (2 × N_{trz}–CH_3), 8.7 (C_{Cp}–CH_3). Anal. calcd. for $C_{23}H_{28}F_6IrN_5O_6S_2$ (840.84): C, 32.85; H, 3.36; N, 8.33 %. Found: C, 32.88; H, 3.15; N, 8.33 %.

Complex 4c: Complex **4a** (60 mg, 0.087 mmol), AgOTf (45 mg, 0.17 mmol) and a drop of water (20 μL, 1.2 mmol) in CH$_2$Cl$_2$ (10 mL) was sonicated during 10 min. at 40 ºC and subsequently stirred for 16 h at room temperature,. The crude mixture was filtered through Celite. Slow evaporation of the filtrate afforded pale yellow crystals that were washed with Et$_2$O (62 mg, 87%). ^1H NMR (500 MHz, D$_2$O) δ 9.14 (d, 1H, $^3J_{HH}$ = 5.5 Hz, H_{py}), 8.31 (t, 1H, $^3J_{HH}$ = 8.0 Hz, H_{py}), 8.22 (d, 1H, $^3J_{HH}$ = 8.0 Hz, H_{py}), 7.76 (t, 1H, $^3J_{HH}$ = 6.6 Hz, H_{py}), 4.59 (s, 3H, $N_{trz}CH_3$), 4.52 (s, 3H, $N_{trz}Me$) 1.80 (s, C_{Cp}–CH_3, 15H). $^{13}C\{^1H\}$NMR (125 MHz, CDCl$_3$) δ 155.2 (C_{trz}–Ir), 153.6 (CH_{py}) 150.0 (C_{qtrz}), 149.0 (C_{qpy}), 141.4 (CH_{py}), 127.2 (CH_{py}), 121.7 (CH_{py}), 90.6 (C_{Cp}), 40.3 (NCH$_3$), 38.5 (NCH$_3$), 8.5 (5 Me). Anal. calcd. for $C_{21}H_{27}F_6IrN_4O_7S_2$: C, 30.88; H, 3.04; N, 6.55. Found: C, 30.84; H, 3.33; N, 6.85.

Complex 5: A mixture of **L5** (100 mg, 0.26 mmol), Ag$_2$O (61 mg, 0.26 mmol), and [Cp*IrCl$_2$]$_2$ (104 mg, 0.13 mmol) in CH$_2$Cl$_2$ (12 mL) was stirred at room temperature for 24 h. After filtration

through Celite, the volume of the filtrate was reduced to ca. 1 mL and excess Et_2O was added. The formed precipitate was isolated and dried, giving **5** as an orange solid (82 mg, 31%). ^1H NMR (CD_3CN, 500 MHz): δ 8.85 (dt, $^3J_{HH}$ = 5.7 Hz, $^4J_{HH}$ = 1.0, Hz, 1H, H_{py}), 8.31–8.29 (m, 2H, H_{py}), 7.82–7.73 (m, 6H, H_{py}+H_{Ph}), 2.67 (s, 3H, C_{trz}–CH_3), 1.83 (s, C_{Cp}–CH_3, 15H). $^{13}C\{^1H\}$ NMR ($CDCl_3$, 125 MHz): δ 152.7 (C_{trz}–Ir), 151.9, 150.5, 142.9, 142.6, 134.7, 132.2, 130.4, 127.9, 125.8, 114.7, 91.8 (C_{Cp}), 30.0 (C_{trz}–CH_3), 8.9 (C_{Cp}–CH_3). Anal. calcd. for $C_{24}H_{27}ClF_6IrN_4P$ (744.13): C, 38.74; H, 3.66; N, 7.53 %. Found: C, 38.59; H, 3.52; N, 7.48 %.

Complex 6a: Compound **L6** (88 mg, 0.24 mmol), Ag_2O (55 mg, 0.24 mmol), and $[Cp*IrCl_2]_2$ (95 mg, 0.12 mmol) were suspended in CH_2Cl_2 (15 mL) and stirred for 18 h. The mixture was filtered through Celite and concentrate to ca. 1 mL. Addition of excess Et_2O resulted in the precipitation of yellow solid, which was isolated and purified by flash chromatography using SiO_2 and CH_2Cl_2/MeCN (1:4 v/v), yielded **6a** as a yellow solid (110 mg, 61%). ^1H NMR ($CDCl_3$, 300 MHz): δ 8.76 (d, $^3J_{HH}$ = 5.8 Hz, 1H, H_{py}), 8.20 (d, $^3J_{HH}$ = 7.8 Hz, 1H, H_{py}), 8.08 (td, $^3J_{HH}$ = 7.8 Hz, $^4J_{HH}$ = 1.4 Hz, 1H, H_{py}), 8.06–8.0 (m, 2H, H_{Ph}), 7.66–7.58 (m, 3H, H_{Ph}), 7.44 (ddd, $^3J_{HH}$ = 7.8 Hz, $^3J_{HH}$ = 5.8 Hz, $^4J_{HH}$ = 1.4 Hz, 1H, H_{py}), 4.71 (s, 3H, N_{trz}–CH_3), 1.47 (s, 15H, C_{Cp}–CH_3). $^{13}C\{^1H\}$ NMR ($CDCl_3$, 125 MHz): δ 155.9 (C_{trz}–Ir), 153.1, 149.3, 148.7, 140.1, 138.1, 130.9, 129.8, 125.8, 125.6, 121.9, 91.1 (C_{Cp}), 39.5 (N_{trz}–CH_3), 8.9 (C_{Cp}–CH_3). Anal. calcd. for $C_{25}H_{27}ClF_3IrN_4O_3S$ (748.24): C, 40.13; H, 3.64; N, 7.49 %. Found: C, 39.98; H, 3.60; N, 7.25 %.

Complex 6b: Complex **6a** (100 mg, 0.134 mmol) was refluxed with AgOTf (52 mg, 0.20 mmol) in MeCN (10 mL) for 24 h. The mixture was filtered through Celite and all volatiles were removed. The residue was washed with $CHCl_3$ (4 × 1 mL) and dried in vacuo, thus affording **6b** as a pale yellow solid (85 mg, 70%). ^1H NMR (CD_3CN, 300 MHz): δ 8.95 (d, $^3J_{HH}$ = 5.8 Hz, 1H, H_{py}), 8.30 (t, $^3J_{HH}$ = 7.8 Hz, 1H, H_{py}), 8.20 (d, $^3J_{HH}$ = 7.8 Hz, 1H, H_{py}), 7.79 (m, 5H, H_{Ph}), 7.73 (dd, $^3J_{HH}$ = 7.8 Hz, $^3J_{HH}$ = 5.8 Hz, 1H, H_{py}), 4.60 (s, 3H, N_{trz}–CH_3), 1.47 (s, 15H, C_{Cp}–CH_3). $^{13}C\{^1H\}$ NMR (CD_3CN, 125 MHz): δ 155.1 (C_{trz}–Ir), 150.1, 149.9, 149.1, 141.6, 137.6, 131.8, 130.6, 127.6, 125.4, 122.4, 93.8 (C_{Cp}), 39.5 (N_{trz}–CH_3), 8.3 (C_{Cp}–CH_3). Anal. calcd. for $C_{28}H_{30}F_6IrN_5O_6S_2$ (902.91): C, 37.25; H, 3.35; N, 7.76 %. Found: C, 37.23; H, 3.22; N, 7.74 %.

Complex 7: A suspension of **L7** (200 mg, 0.364 mmol), Ag_2O (84 mg, 0.36 mmol), and $[Cp*IrCl_2]_2$ (144 mg, 0.18 mmol) in MeCN (25 mL) was refluxed for 24 h. The mixture was filtered through Celite under an N_2 atmosphere and the volatiles were removed. The residue was dissolved in CH_2Cl_2 and filtered again through Celite, concentrated to ca. 1 mL and treated with excess Et_2O. The formed precipitate was collected and dried in vacuo, yielding **7** a yellow solid (120 mg, 33%). ^1H NMR (CD_3CN, 600 MHz): δ 9.18 (d, $^3J_{HH}$ = 6.2 Hz, 1H, H_{py}), 8.83 (t, $^3J_{HH}$ = 7.9, 1H, H_{py}), 8.49 (dd, $^3J_{HH}$ = 7.9 Hz, $^4J_{HH}$ = 1.3 Hz, 1H, H_{py}), 8.35 (ddd, $^3J_{HH}$ = 7.9 Hz, $^3J_{HH}$ = 6.2 Hz, $^4J_{HH}$ = 1.3 Hz, 1H, H_{py}), 7.85 (dd, $^3J_{HH}$ = 7.6 Hz, $^4J_{HH}$ = 1.4 Hz, 1H, H_{Ph}), 7.81 (d, $^3J_{HH}$ = 7.6 Hz, $^4J_{HH}$ = 1.4 Hz, 1H, H_{Ph}), 7.35, 7.30 (2 × td, $^3J_{HH}$ = 7.6 Hz, $^4J_{HH}$ = 1.4 Hz, 12H, H_{Ph}), 4.34 (s, 3H, N_{py}–CH_3), 4.19 (s, 3H, N_{trz}–CH_3), 1.57 (s, 15H, C_{Cp}–CH_3). $^{13}C\{^1H\}$ NMR ($CDCl_3$, 125 MHz): δ 149.4, 147.6, 146.6 (C_{trz}–Ir), 144.1(C_{Ph}–Ir), 141.8, 138.0, 137.3,

135.5, 133.4, 130.3, 130.1, 124.8, 114.4, 93.4 (C_{Cp}), 47.9 (N_{py}–CH_3), 38.6 (N_{trz}–CH_3), 8.4 (C_{Cp}–CH_3). Anal. calcd. for $C_{29}H_{32}F_6IrN_5O_6S_2$ (916.93): C, 37.99; H, 3.52; N, 7.64 %. Found: C, 37.57; H, 3.50; N, 7.42 %.

Complex 8: A suspension containing **L8** (86 mg, 0.18 mmol), Ag_2O (41 mg, 0.18 mmol), and $[Cp*IrCl_2]_2$ (71 mg, 0.09 mmol) in MeCN (10 mL) was refluxed for 24 h. The mixture was filtered through Celite and the filtrate was concentrated to ca. 1 mL. Excess Et_2O was added and the formed precipitate was collected and dried, yielding **8** as a yellow solid (72 mg, 40%). ^1H NMR (CD_3CN, 500 MHz): δ 8.71 (d, $^3J_{HH}$ = 7.6 Hz, 1H, H_{py}), 8.30 (d, $^3J_{HH}$ = 6.1 Hz, 1H, H_{py}), 7.51 (dd, $^3J_{HH}$ = 7.6 Hz, $^3J_{HH}$ = 6.1 Hz, 1H, H_{py}), 4.61 (s, 3H, N_{trz}–CH_3), 4.59 (s, 3H, N_{py}–CH_3), 4.32 (s, 3H, N_{trz}–CH_3), 1.84 (s, 15H, C_{Cp}–CH_3). $^{13}C\{^1H\}$ NMR (CD_3CN, 100 MHz): δ 154.6 (C_{trz}–Ir), 154.0 (C_{py}–Ir), 152.9, 152.6, 148.7, 139.9, 125.2, 110.2 (NCCH_3), 94.6 (C_{Cp}), 49.6 (N_{trz}–CH_3), 43.8 (N_{py}–CH_3), 39.9 (N_{trz}–CH_3), 8.8 (C_{Cp}–CH_3), 4.6 (NCCH_3). Anal. calcd. for $C_{24}H_{30}F_6IrN_5O_6S_2$ (854.86): C, 33.72; H, 3.54; N, 8.19 %. Found: C, 33.59; H, 3.52; N, 7.92 %.

Dynamic Oxygen Evolution Measurement: Complexes were investigated for water oxidation by mixing them with ceric ammonium nitrate (CAN) in water buffered with 1N nitric acid with pressure monitoring and GC analysis as previously described.[18] Extended reactivity experiments were conducted in 20/40/60 mL EPA vials as well as sealed cuvettes enabling concurrent UV/vis spectroscopy.

Time-dependent DFT (TD-DFT). Geometry optimizations were performed using the unrestricted B3LYP functional with the 6-31G(2d,2p) basis set for C, N, O, and H and LANL2DZ for Ir. Optimizations were conducted with solvent water using the continuous polarizable continuum model as implemented in Gaussian 09 Rev. D. Time dependent calculations were performed at the optimized ground-state geometry using the LANL2DZ basis set since that basis set has previously resulted in superior agreement of TD-DFT spectra with experimental data[83]. The energy and oscillator strength were computed for each of the 150 lowest excitations and electronic transitions were expanded as Gaussian curves with a FWHM (full width at half- maximum) for each peak set to 0.372 eV (3000 cm^{-1}).[84]

Crystal structure determinations. Crystal data were collected using an Oxford Diffraction SuperNova A diffractometer fitted with an Atlas detector. Crystals were measured with monochromated Mo-K_α radiation (0.71073 Å). A twice redundant dataset was collected, assuming that the Friedel pairs are not equivalent. An analytical absorption correction based on the shape of the crystal was performed.[85] The structures were solved by direct methods using SHELXS-97 and refined by full matrix least-squares on F^2 for all data using SHELXL-97.[86] Hydrogen atoms were added at calculated positions and refined using a riding model. Their isotropic temperature factors were fixed to 1.2 times (1.5 times for methyl groups) the equivalent isotropic displacement parameters of the carbon atom the H-atom is attached to. Anisotropic thermal displacement parameters were used for all non-hydrogen atoms. Further crystallographic details are compiled in the Supporting Information. CCDC 850692–850700 contain the supplementary crystallographic data for this paper. These data can be obtained free of charge from the Cambridge Crystallographic Data Centre via www.ccdc.cam.ac.uk/data_request/cif.

Notes and references

(1) *EIA - 2012 International Energy Outlook*; 2012.
(2) Kiehl, J. T.; Trenberth, K. E. *Bull. Am. Meteorol. Soc.* **1997**, *78*, 197–208.
(3) McDaniel, N. D.; Bernhard, S. *Dalt. Trans.* **2010**, *39*, 10021–10030.
(4) Brooks, A. C.; Basore, K.; Bernhard, S. *Inorg. Chem.* **2013**, *52*, 5794–5800.
(5) Cline, E. D.; Adamson, S. E.; Bernhard, S. *Inorg. Chem.* **2008**, *47*, 10378–10388.
(6) Seshadri, G.; Lin, C.; Bocarsly, A. B. *J. Electroanal. Chem.* **1994**, *372*, 145–150.
(7) Gersten, S. W.; Samuels, G. J.; Meyer, T. J. *J. Am. Chem. Soc.* **1982**, *104*, 4029–4030.
(8) Gilbert, J. A.; Eggleston, D. S.; Murphy, W. R.; Geselowitz, D. A.; Gersten, S. W.; Hodgson, D. J.; Meyer, T. J. *J. Am. Chem. Soc.* **1985**, *107*, 3855–3864.
(9) Sens, C.; Romero, I.; Rodríguez, M.; Llobet, A.; Parella, T.; Benet-Buchholz, J. *J. Am. Chem. Soc.* **2004**, *126*, 7798–7799.
(10) Zong, R.; Thummel, R. P. *J. Am. Chem. Soc.* **2005**, *127*, 12802–12803.
(11) Sartorel, A.; Carraro, M.; Scorrano, G.; De Zorzi, R.; Geremia, S.; McDaniel, N. D.; Bernhard, S.; Bonchio, M. *J. Am. Chem. Soc.* **2008**, *130*, 5006–5007.
(12) Sartorel, A.; Miró, P.; Salvadori, E.; Romain, S.; Carraro, M.; Scorrano, G.; Di Valentin, M.; Llobet, A.; Bo, C.; Bonchio, M. *J. Am. Chem. Soc.* **2009**, *131*, 16051–16053.
(13) Geletii, Y. V; Botar, B.; Kögerler, P.; Hillesheim, D. A.; Musaev, D. G.; Hill, C. L. *Angew. Chemie, Int. Ed.* **2008**, *47*, 3896–3899.
(14) Yin, Q.; Tan, J. M.; Besson, C.; Geletii, Y. V; Musaev, D. G.; Kuznetsov, A. E.; Luo, Z.; Hardcastle, K. I.; Hill, C. L. *Science* **2010**, *328*, 342–345.
(15) McCool, N. S.; Robinson, D. M.; Sheats, J. E.; Dismukes, G. C. *J. Am. Chem. Soc.* **2011**, *133*, 11446–11449.
(16) Limburg, J.; Vrettos, J. S.; Chen, H.; de Paula, J. C.; Crabtree, R. H.; Brudvig, G. W. *J. Am. Chem. Soc.* **2001**, *123*, 423–430.
(17) Tseng, H.-W.; Zong, R.; Muckerman, J. T.; Thummel, R. *Inorg. Chem.* **2008**, *47*, 11763–11773.
(18) McDaniel, N. D.; Coughlin, F. J.; Tinker, L. L.; Bernhard, S. *J. Am. Chem. Soc.* **2008**, *130*, 210–217.
(19) Concepcion, J. J.; Jurss, J. W.; Templeton, J. L.; Meyer, T. J. *J. Am. Chem. Soc.* **2008**, *130*, 16462–16463.
(20) Kohl, S. W.; Weiner, L.; Schwartsburd, L.; Konstantinovski, L.; Shimon, L. J. W.; Ben-David, Y.; Iron, M. A.; Milstein, D. *Science* **2009**, *324*, 74–77.
(21) Ellis, W. C.; McDaniel, N. D.; Bernhard, S.; Collins, T. J. *J. Am. Chem. Soc.* **2010**, *132*, 10990–10991.
(22) Bernet, L.; Lalrempuia, R.; Ghattas, W.; Mueller-Bunz, H.; Vigara, L.; Llobet, A.; Albrecht, M. *Chem. Commun.* **2011**, *47*, 8058–8060.
(23) Savini, A.; Bellachioma, G.; Bolaño, S.; Rocchigiani, L.; Zuccaccia, C.; Zuccaccia, D.; Macchioni, A. *ChemSusChem* **2012**, *5*, 1415–1419.
(24) Duan, L.; Bozoglian, F.; Mandal, S.; Stewart, B.; Privalov, T.; Llobet, A.; Sun, L. *Nat. Chem.* **2012**, *4*, 418–423.
(25) Hull, J. F.; Balcells, D.; Blakemore, J. D.; Incarvito, C. D.; Eisenstein, O.; Brudvig, G. W.; Crabtree, R. H. *J. Am. Chem. Soc.* **2009**, *131*, 8730–8731.
(26) Lalrempuia, R.; McDaniel, N. D.; Müller-Bunz, H.; Bernhard, S.; Albrecht, M. *Angew. Chemie, Int. Ed.* **2010**, *49*, 9765–9768.
(27) Blakemore, J. D.; Schley, N. D.; Balcells, D.; Hull, J. F.; Olack, G. A.; Incarvito, C. D.; Eisenstein, O.; Brudvig, G. W.; Crabtree, R. H. *J. Am. Chem. Soc.* **2010**, *132*, 16017–16029.
(28) Savini, A.; Bellachioma, G.; Ciancaleoni, G.; Zuccaccia, C.; Zuccaccia, D.; Macchioni, A. *Chem. Commun.* **2010**, *46*, 9218–9219.
(29) Hetterscheid, D. G. H.; Reek, J. N. H. *Chem. Commun.* **2011**, *47*, 2712–2714.
(30) Savini, A.; Belanzoni, P.; Bellachioma, G.; Zuccaccia, C.; Zuccaccia, D.; Macchioni, A. *Green Chem.* **2011**, *13*, 3360–3374.
(31) Grotjahn, D. B.; Brown, D. B.; Martin, J. K.; Marelius, D. C.; Abadjian, M.-C.; Tran, H. N.; Kalyuzhny, G.; Vecchio, K. S.; Specht, Z. G.; Cortes-Llamas, S. A.; Miranda-Soto, V.; van Niekerk, C.; Moore, C. E.; Rheingold, A. L. *J. Am. Chem. Soc.* **2011**, *133*, 19024–19027.
(32) Hong, D.; Murakami, M.; Yamada, Y.; Fukuzumi, S. *Energy Environ. Sci.* **2012**, *5*, 5708–5716.
(33) Junge, H.; Marquet, N.; Kammer, A.; Denurra, S.; Bauer, M.; Wohlrab, S.; Gärtner, F.; Pohl, M.-M.; Spannenberg, A.; Gladiali, S.; Beller, M. *Chem. - A Eur. J.* **2012**, *18*, 12749–12758.
(34) Schley, N. D.; Blakemore, J. D.; Subbaiyan, N. K.; Incarvito, C. D.; D'Souza, F.; Crabtree, R. H.; Brudvig, G. W. *J. Am. Chem. Soc.* **2011**, *133*, 10473–10481.
(35) DeKrafft, K. E.; Wang, C.; Xie, Z.; Su, X.; Hinds, B. J.; Lin, W. *ACS Appl. Mater. Interfaces* **2012**, *4*, 608–613.
(36) Youngblood, W. J.; Lee, S.-H. A.; Maeda, K.; Mallouk, T. E. *Acc. Chem. Res.* **2009**, *42*, 1966–1973.
(37) Herrero, C.; Quaranta, A.; Leibl, W.; Rutherford, A. W.; Aukauloo, A. *Energy Environ. Sci.* **2011**, *4*, 2353.
(38) Moore, G. F.; Blakemore, J. D.; Milot, R. L.; Hull, J. F.; Song, H.; Cai, L.; Schmuttenmaer, C. A.; Crabtree, R. H.; Brudvig, G. W. *Energy Environ. Sci.* **2011**, *4*, 2389.
(39) Reece, S. Y.; Hamel, J. A.; Sung, K.; Jarvi, T. D.; Esswein, A. J.; Pijpers, J. J. H.; Nocera, D. G. *Science* **2011**, *334*, 645–648.
(40) Raubenheimer, H. G.; Cronje, S. *Dalt. Trans.* **2008**, 1265–1272.
(41) Mathew, P.; Neels, A.; Albrecht, M. *J. Am. Chem. Soc.* **2008**, *130*, 13534–13535.
(42) Guisado-Barrios, G.; Bouffard, J.; Donnadieu, B.; Bertrand, G. *Angew. Chemie, Int. Ed.* **2010**, *49*, 4759–4762.
(43) Poulain, A.; Canseco-Gonzalez, D.; Hynes-Roche, R.; Müller-Bunz, H.; Schuster, O.; Stoeckli-Evans, H.; Neels, A.; Albrecht, M. *Organometallics* **2011**, *30*, 1021–1029.
(44) Saravanakumar, R.; Ramkumar, V.; Sankararaman, S. *Organometallics* **2011**, *30*, 1689–1694.
(45) Albrecht, M. *Chem. Rev.* **2010**, *110*, 576–623.
(46) Tulchinsky, Y.; Iron, M. A.; Botoshansky, M.; Gandelman, M. *Nat. Chem.* **2011**, *3*, 525–531.
(47) Chianese, A. R.; Kovacevic, A.; Zeglis, B. M.; Faller, J. W.; Crabtree, R. H. *Organometallics* **2004**, *23*, 2461–2468.
(48) Heckenroth, M.; Kluser, E.; Neels, A.; Albrecht, M. *Angew. Chemie, Int. Ed.* **2007**, *46*, 6293–6296.
(49) Ung, G.; Bertrand, G. *Chem. - A Eur. J.* **2011**, *17*, 8269–8272.
(50) Araki, S.; Wanibe, Y.; Uno, F.; Morikawa, A.; Yamamoto, K.; Chiba, K.; Butsugan, Y. *Chem. Ber.* **1993**, *126*, 1149–1155.
(51) Albrecht, M. *Chem. Commun.* **2008**, 3601–3610.
(52) Schuster, O.; Yang, L.; Raubenheimer, H. G.; Albrecht, M. *Chem. Rev.* **2009**, *109*, 3445–3478.
(53) Melaimi, M.; Soleilhavoup, M.; Bertrand, G. *Angew. Chemie, Int. Ed.* **2010**, *49*, 8810–8849.
(54) Complex **11** was isolated as a minor fraction from column purification of complex **4a** by changing the mobile phase after elution of **4a** from CH_2Cl_2/MeCN to pure MeOH. ^1H NMR data for **11** (CD_3CN, 300 MHz): δ 8.71 (d, $^3J_{HH}$ = 4.2 Hz, 1H, H$_{py}$), 7.95–7.83 (m, 3H, H$_{py}$), 7.79 (t, $^3J_{HH}$ = 7.8 Hz, 1H, H$_{py}$), 7.65–7.58 (m, 1H, H$_{py}$), 6.91–6.78 (m, 2H, H$_{py}$), 4.37, 4.23, 4.05, 3.55 (4 × s, 3H, N$_{trz}$–CH3), 1.80 (s, 15H, C$_{Cp}$–CH3).
(55) Poyatos, M.; Mata, J. A.; Peris, E. *Chem. Rev.* **2009**, *109*, 3677–3707.
(56) Binstead, R. A.; Meyer, T. J. *J. Am. Chem. Soc.* **1987**, *109*, 3287–3297.
(57) Yu, P.; O'Keefe, T. J. *J. Electrochem. Soc.* **2006**, *153*, C80.
(58) Ikeda-Ohno, A.; Tsushima, S.; Hennig, C.; Yaita, T.; Bernhard, G. *Dalt. Trans.* **2012**, *41*, 7190–7192.

(59) Hintermair, U.; Hashmi, S. M.; Elimelech, M.; Crabtree, R. H. *J. Am. Chem. Soc.* **2012**, *134*, 9785–9795.

(60) Petronilho, A.; Rahman, M.; Woods, J. A.; Al-Sayyed, H.; Müller-Bunz, H.; Don MacElroy, J. M.; Bernhard, S.; Albrecht, M. *Dalt. Trans.* **2012**, *41*, 13074–13080.

(61) Barnett, S. M.; Goldberg, K. I.; Mayer, J. M. *Nat. Chem.* **2012**, *4*, 498–502.

(62) Crabtree, R. H. *Chem. Rev.* **2012**, *112*, 1536–1554.

(63) Petronilho, A.; Woods, J. A.; Bernhard, S.; Albrecht, M. *Eur. J. Inorg. Chem.* **2014**, *2014*, 708–714.

(64) Graeupner, J.; Hintermair, U.; Huang, D. L.; Thomsen, J. M.; Takase, M.; Campos, J.; Hashmi, S. M.; Elimelech, M.; Brudvig, G. W.; Crabtree, R. H. *Organometallics* **2013**, *32*, 5384–5390.

(65) Fogler, H. S. *Elements of Chemical Reaction Engineering (4th Edition)*; Prentice Hall, 2005; p. 1080.

(66) Wasylenko, D. J.; Ganesamoorthy, C.; Henderson, M. A.; Berlinguette, C. P. *Inorg. Chem.* **2011**, *50*, 3662–3672.

(67) Yoshida, M.; Masaoka, S.; Abe, J.; Sakai, K. *Chem. - An Asian J.* **2010**, *5*, 2369–2378.

(68) Kimoto, A.; Yamauchi, K.; Yoshida, M.; Masaoka, S.; Sakai, K. *Chem. Commun.* **2012**, *48*, 239–241.

(69) Codolà, Z.; Garcia-Bosch, I.; Acuña-Parés, F.; Prat, I.; Luis, J. M.; Costas, M.; Lloret-Fillol, J. *Chem. - A Eur. J.* **2013**, *19*, 8042–8047.

(70) Blakemore, J. D.; Schley, N. D.; Olack, G. W.; Incarvito, C. D.; Brudvig, G. W.; Crabtree, R. H. *Chem. Sci.* **2011**, *2*, 94.

(71) Castillo-Blum, S. E.; Richens, D. T.; Sykes, A. G. *Inorg. Chem.* **1989**, *28*, 954–960.

(72) Hintermair, U.; Sheehan, S. W.; Parent, A. R.; Ess, D. H.; Richens, D. T.; Vaccaro, P. H.; Brudvig, G. W.; Crabtree, R. H. *J. Am. Chem. Soc.* **2013**.

(73) Blackmond, D. G. *Angew. Chemie, Int. Ed.* **2005**, *44*, 4302–4320.

(74) Malinowski, E. R. *Factor Analysis in Chemistry*; Wiley, 2002.

(75) Mason, C.; Maeder, M.; Whitson, A. *Anal. Chem.* **2001**, *73*, 1587–1594.

(76) Maeder, M.; Neuhold, Y.-M. *Practical Data Analysis in Chemistry, Volume 26 (Data Handling in Science and Technology)*; Elsevier Science, 2007; p. 340.

(77) Codolà, Z.; M S Cardoso, J.; Royo, B.; Costas, M.; Lloret-Fillol, J. *Chem. - A Eur. J.* **2013**, *19*, 7203–7213.

(78) Zuccaccia, C.; Bellachioma, G.; Bolaño, S.; Rocchigiani, L.; Savini, A.; Macchioni, A. *Inorg. Chem.* **2012**, *2012*, 1462–1468.

(79) Krüger, A.; Albrecht, M. *Aust. J. Chem.* **2011**, *64*, 1113.

(80) Hammarström, L.; Styring, S. *Energy Environ. Sci.* **2011**, *4*, 2379.

(81) Ykman, P.; L'abbé, G.; Smets, G. *Tetrahedron* **1971**, *27*, 845–849.

(82) Ball, R. G.; Graham, W. A. G.; Heinekey, D. M.; Hoyano, J. K.; McMaster, A. D.; Mattson, B. M.; Michel, S. T. *Inorg. Chem.* **1990**, *29*, 2023–2025.

(83) Coughlin, F. J.; Westrol, M. S.; Oyler, K. D.; Byrne, N.; Kraml, C.; Zysman-Colman, E.; Lowry, M. S.; Bernhard, S. *Inorg. Chem.* **2008**, *47*, 2039–2048.

(84) O'Boyle, N. M.; Tenderholt, A. L.; Langner, K. M. *J. Comput. Chem.* **2008**, *29*, 839–845.

(85) Version, P. C. Program CrysalisPro Version 1.171.33.55, Oxford Diffraction Limited, 2010.

(86) Sheldrick, G. M. *Acta Crystallogr. Sect. A Found. Crystallogr.* **2008**, *64*, 112–122.
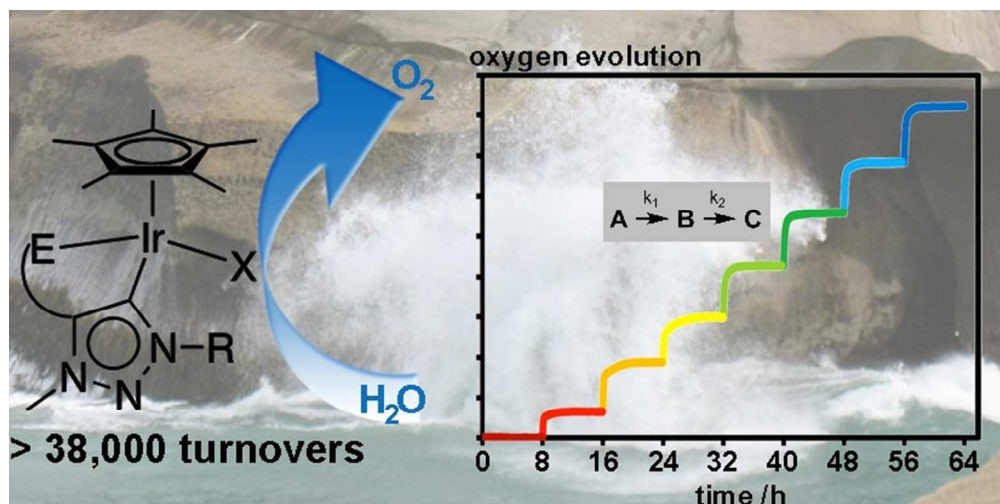
Combined kinetic & in operando spectroscopic studies, factor analysis, and DFT calculations provide insight into the water oxidation reaction catalyzed by operationally homogeneous iridium mesoionic carbene complexes.
70x34mm (300 x 300 DPI)